Pulsar Timing Array Constraints on Primordial Black Holes with NANOGrav 11-Year Dataset

Zu-Cheng Chen,[1,2,3,*] Chen Yuan,[1,2,†] and Qing-Guo Huang[1,2,4,5,6,‡]

[1]CAS Key Laboratory of Theoretical Physics, Institute of Theoretical Physics, Chinese Academy of Sciences, Beijing 100190, China
[2]School of Physical Sciences, University of Chinese Academy of Sciences, No. 19A Yuquan Road, Beijing 100049, China
[3]School of Physics and Astronomy, Cardiff University, Cardiff CF24 3AA, United Kingdom
[4]School of Fundamental Physics and Mathematical Sciences Hangzhou Institute for Advanced Study, UCAS, Hangzhou 310024, China
[5]Center for Gravitation and Cosmology, College of Physical Science and Technology, Yangzhou University, Yangzhou 225009, China
[6]Synergetic Innovation Center for Quantum Effects and Applications, Hunan Normal University, Changsha 410081, China

(Received 30 January 2020; accepted 29 May 2020; published 22 June 2020)

The detection of binary black hole coalescences by LIGO and Virgo has aroused the interest in primordial black holes (PBHs), because they could be both the progenitors of these black holes and a compelling candidate of dark matter (DM). PBHs are formed soon after the enhanced scalar perturbations reenter horizon during the radiation dominated era, which would inevitably induce gravitational waves as well. Searching for such scalar induced gravitational waves (SIGWs) provides an elegant way to probe PBHs. We perform the first direct search for the signals of SIGWs accompanying the formation of PBHs in the North American Nanohertz Observatory for Gravitational waves (NANOGrav) 11-year dataset. No statistically significant detection has been made, and hence we place a stringent upper limit on the abundance of PBHs at 95% confidence level. In particular, less than one part in a million of the total DM mass could come from PBHs in the mass range of $[2 \times 10^{-3}, 7 \times 10^{-1}]\ M_{\odot}$.

DOI: 10.1103/PhysRevLett.124.251101

Introduction.—Over the past few years, the great achievement of detecting gravitational waves (GWs) from binary black holes (BBHs) [1–7] and a binary neutron star (BNS) [8] by LIGO and Virgo has led us to the era of GW astronomy, as well as the era of multimessenger astronomy. Various models have been proposed to account for the formation and evolution of these LIGO and Virgo BBHs, among which the primordial black hole (PBH) scenario [9–11] has attracted a lot of attention recently. PBHs are predicted to undergo gravitational collapse from overdensed regions in the infant Universe [12,13] when the corresponding wavelength of enhanced scalar curvature perturbations reenter the horizon [14–18].

The PBH scenario is appealing because it can not only account for the event rate of LIGO and Virgo BBHs, but also be a promising candidate for the long elusive missing part of our Universe—dark matter (DM). It is inconclusive that whether PBHs can represent all DM or not, yet the abundance of PBHs (f_{PBH}) which describes the total DM mass in the form of PBHs, has been constrained by a variety of observations, such as extragalactic γ rays from PBH evaporation [19], femtolensing of γ-ray bursts [20], Subaru HSC microlensing [21], Kepler milli- and microlensing [22], OGLE microlensing [23], EROS and MACHO microlensing [24], existence of white dwarfs (WDs) which are not triggered to explode in our local galaxy [25] (this constraint might be ineffective according to the simulation in [26]), dynamical heating of ultrafaint dwarf galaxies [27], x-ray and radio emission from the accretion of interstellar gas onto PBHs [28], cosmic microwave background radiation from the accretion of primordial gas onto PBHs [29–32], and GWs either through the null detection of subsolar mass BBHs [33–36] or the null detection of stochastic GW background (SGWB) from BBHs [35,37]. But PBHs in a substantial window in the approximate mass range $[10^{-16}, 10^{-14}] \cup [10^{-13}, 10^{-12}]\ M_{\odot}$ are still allowed to account for all of the DM. We refer to Ref. [35] for a recent summary.

Actually there is another way to probe the PBH DM scenario, namely through the scalar induced GWs (SIGWs) which would inevitably be generated in conjunction with the formation of PBHs [38–44]. The feature for distinguishing SIGWs from other sources was sketched out in Ref. [45] recently. Since PBHs are supposed to form from the tail of the probability density function of the curvature perturbations, the possibility to form a single PBH is quite sensitive to the amplitude of curvature perturbation power spectrum [40]. Consequently the abundance of PBHs is extremely sensitive to the amplitude of the corresponding SIGW. Therefore a detection of SIGWs will provide evidence for PBHs, while the null detection of SIGWs will put a stringent constraint on the abundance of PBHs.

The peak frequency of the SIGW (f_*) is determined by the peak wave mode of the comoving curvature power spectrum, and thus is related to the mass of PBHs by $f_* \sim 3\ \mathrm{Hz}(m_{\mathrm{PBH}}/10^{-18}\ M_{\odot})^{-1/2}$ [39]. The mass of PBHs

constituting DM should be heavier than $10^{-18}\ M_\odot$, otherwise they would have evaporated due to Hawking radiation. As a result, the corresponding peak frequency of the SIGW should be lower than 3 Hz, and then it is difficult for the ground-based detectors like LIGO and Virgo to detect the corresponding SIGWs. On the other hand, the GW observatories hunting for low frequency signals are especially suitable to explore the PBH DM hypothesis, and the prospective constraints on the abundance of PBHs by LISA [46] and pulsar timing observations such as IPTA [47], FAST [48], and SKA [49] have been investigated in Ref. [42]. See some other related works in Refs. [43,50–55].

Although the data of current pulsar timing array (PTA) has been used to constrain the amplitude of SGWBs, those results strongly depend on the assumption of some special power-law form which is quite different from SIGWs [42]. Therefore, in this Letter, we perform the first search in the public available PTA dataset for the signal of SIGWs in order to test the PBH DM hypothesis. In particular, the null detection of SIGWs in the current NANOGrav 11-year dataset [56] provides a constraint on the abundance of PBHs through SIGWs in the mass range of $[4\times10^{-4}, 1.7]\ M_\odot$.

PBH, DM, and SIGW.—In this Letter, we consider the monochromatic formation of PBHs, corresponding to a δ power spectrum of the scalar curvature perturbation, i.e.,

$$\mathcal{P}_\zeta(f) = A f_* \delta(f - f_*), \tag{1}$$

where A is the dimensionless amplitude of the power spectrum. In this case, the mass of the PBHs is related to the peak frequency f_* by [12,13]

$$\frac{m_{\rm PBH}}{M_\odot} \simeq 2.3\times10^{18}\left(\frac{H_0}{f_*}\right)^2, \tag{2}$$

where f_* is in units of Hz, and H_0 is the Hubble constant. The formation of a PBH is a threshold process which is described by three-dimensional statistics of Gaussian random fields, also known as peak theory [57], and the abundance of PBHs in DM, $f_{\rm PBH}\equiv\Omega_{\rm PBH}/\Omega_{\rm DM}$, is given by [58]

$$f_{\rm PBH} \simeq 1.9\times10^7(\zeta_c^2/A-1)e^{-\frac{\zeta_c^2}{2A}}\left(\frac{m_{\rm PBH}}{M_\odot}\right)^{-\frac{1}{2}}, \tag{3}$$

where $\zeta_c \simeq 1$ [59–64] is the threshold value for the formation of PBHs.

In Ref. [65] the energy density of a GW background $\rho_{\rm GW}$ takes the form

$$\rho_{\rm GW} = \int \rho_{\rm GW}(f,\eta) d\ln f = \frac{M_p^2}{16a^2}\overline{\langle \partial_k h_{ij}\partial^k h^{ij}\rangle}, \tag{4}$$

where η is the conformal time, a is the scale factor, M_p is the Planck mass, and the overline stands for time average. It is useful to introduce the dimensionless GW energy density parameter per logarithm frequency $\Omega_{\rm GW}(\eta,k)$ defined by

$$\Omega_{\rm GW}(\eta,f) \equiv \frac{\rho_{\rm GW}(f,\eta)}{\rho_{\rm cr}}, \tag{5}$$

where $\rho_{\rm cr}$ is the critical energy of the present Universe. For a monochromatic formation of PBHs, the present $\Omega_{\rm GW}(f)$ of the SIGW in radiation dominated era can be estimated as [42]

$$\Omega_{\rm GW}(f) = \Omega_{\rm GW}^{(2)}(f) + \Omega_{\rm GW}^{(3)}(f). \tag{6}$$

Here, the leading order contribution $\Omega_{\rm GW}^{(2)}(f)$ is given by [66,67]

$$\begin{aligned}\Omega_{\rm GW}^{(2)}(f) = {}& \frac{3\tilde{f}^2A^2}{1024}\Omega_r(4-\tilde{f}^2)^2(3\tilde{f}^2-2)^2\Theta(2-\tilde{f}) \\ & \times\left[\pi^2(3\tilde{f}^2-2)^2\Theta(2\sqrt{3}-3\tilde{f})\right. \\ & \left.+\left(4+(3\tilde{f}^2-2)\log\left|1-\frac{4}{3\tilde{f}^2}\right|\right)^2\right],\end{aligned} \tag{7}$$

where $\tilde{f}\equiv f/f_*$ is the dimensionless frequency and Θ is the Heaviside theta function. In addition, the third-order correction $\Omega_{\rm GW}^{(3)}(f)$ reads [42]

$$\Omega_{\rm GW}^{(3)}(f) = \frac{A^3}{384\tilde{f}^2}\Omega_r(M_2\overline{I_3^2} + M_1\overline{I_2 I_4}). \tag{8}$$

The definitions of M_1, M_2, I_2, I_3, and I_4 are complicated and can be found in Ref. [42].

PTA data analysis.—Null detection of certain GW backgrounds has been reported by the current PTAs such as NANOGrav [68], PPTA [69], and EPTA [70], and the upper bounds on the amplitude of those GW backgrounds have also been continually improved. For instance, NANOGrav has constrained on the SGWB produced by supermassive black holes [71] and other types of spectra [72] such as power-law, broken-power-law, free and Gaussian-process-interpolated spectra. Similar studies were also performed by the PPTA Collaboration [73] and the EPTA Collaboration [74]. In this Letter we search for the signal of SIGWs using the NANOGrav 11-year dataset which consists of time of arrival (TOA) data and pulsar timing models presented in Ref. [56]. Similar to Ref. [75], we choose six pulsars which have relatively good TOA precision and long observation time. A summary of the basic properties of these pulsars is presented in Table I. For all the six pulsars, $T_{\rm obs}$ is longer than 8 yr, $N_{\rm TOA}$ is more than 10^4, and rms (root-mean-square) is less than 1.5 μs.

TABLE I. Basic properties of the six pulsars used in our analysis: rms—the weighted root-mean-square epoch-averaged post-fit timing residuals, $N_{\rm epoch}$—number of observational epochs, $N_{\rm TOA}$—number of TOAs, $T_{\rm obs}$—observational time span. See Ref. [56] in detail.

Pulsar name	rms [μs]	$N_{\rm epoch}$	$N_{\rm TOA}$	$T_{\rm obs}$ [yr]
J0613 − 0200	0.422	324	11 566	10.8
J1012 + 5307	1.07	493	16 782	11.4
J1600 − 3053	0.23	275	12 433	8.1
J1713 + 0747	0.108	789	27 571	10.9
J1744 − 1134	0.842	322	11 550	11.4
J1909 − 3744	0.148	451	17 373	11.2

The presence of a GW background will manifest as the unexplained residuals in the TOAs of pulsar signals after subtracting a deterministic timing model that accounts for the pulsar spin behavior and the geometric effects due to the motion of the pulsar and the Earth [76,77]. It is therefore feasible to separate GW-induced residuals, which have distinctive correlations among different pulsars [78], from other systematic effects, such as clock errors or delays due to light propagation through interstellar medium, by regularly monitoring TOAs of pulsars from an array of the most rotational stable millisecond pulsars [79]. An $N_{\rm TOA}$ length vector $\delta\boldsymbol{t}$ representing the timing residuals for a single pulsar can be modeled as follows [80,81]:

$$\delta\boldsymbol{t} = \boldsymbol{M}\boldsymbol{\epsilon} + \delta\boldsymbol{t}_{\rm RGP}, \tag{9}$$

where $\boldsymbol{M}$ is the timing model design matrix, $\boldsymbol{\epsilon}$ is a vector denoting small offsets for the timing model parameters, and $\boldsymbol{M}\boldsymbol{\epsilon}$ is the residual due to inaccuracies of the timing model. The timing model design matrix is obtained through the LIBSTEMPO [82] package which is a PYTHON interface to TEMPO2 [83] [84,85] timing software. The term $\delta\boldsymbol{t}_{\rm RGP}$ in Eq. (9) is the stochastic contribution to the TOAs, which can be modeled by a sum of random Gaussian processes [86] as

$$\delta\boldsymbol{t}_{\rm RGP} = \delta\boldsymbol{t}_{\rm RN} + \delta\boldsymbol{t}_{\rm WN} + \delta\boldsymbol{t}_{\rm SSE} + \delta\boldsymbol{t}_{\rm SIGW}. \tag{10}$$

The first term on the right-hand side of Eq. (10), $\delta\boldsymbol{t}_{\rm RN}$, represents the red noise via a Fourier decomposition,

$$\delta\boldsymbol{t}_{\rm RN} = \sum_{j=1}^{N_{\rm mode}} \left[a_j \sin\left(\frac{2\pi j t}{T}\right) + b_j \cos\left(\frac{2\pi j t}{T}\right) \right] = \boldsymbol{F}\boldsymbol{a}, \tag{11}$$

where $N_{\rm mode}$ is the number of frequency modes included in the sum, T is the total observation time span, $\boldsymbol{F}$ is the Fourier design matrix with components of alternating sine and cosine functions for frequencies in the range $[1/T, N_{\rm mode}/T]$, and $\boldsymbol{a}$ is a vector giving the amplitude of the Fourier basis functions. In the analysis, we choose $N_{\rm mode} = 50$. The covariant matrix of the red noise coefficients $\boldsymbol{a}$ at frequency modes i and j will be diagonal, namely,

$$\langle \boldsymbol{a}_i \boldsymbol{a}_j \rangle = P(f_i)\delta_{ij}, \tag{12}$$

where the power spectrum $P(f)$ is usually well described by a power-law model,

$$P(f) = \frac{A_{\rm RN}^2}{12\pi^2}\left(\frac{f}{\rm yr^{-1}}\right)^{3-\gamma_{\rm RN}} f^{-3}, \tag{13}$$

with $A_{\rm RN}$ and $\gamma_{\rm RN}$ the amplitude and spectral index of the power law, respectively. Note that in Eq. (12), f_i is defined by i/T if i is odd, and $(i-1)/T$ if i is even.

The second term, $\delta\boldsymbol{t}_{\rm WN}$, accounts for the influence of white noise on the timing residuals, including a scale parameter on the TOA uncertainties (EFAC), an added variance (EQUAD) and a per-epoch variance (ECORR) for each backend and receiver system. This white noise is assumed to follow Gaussian distribution and can be characterized by a covariance matrix as

$$\boldsymbol{C}_{\rm WN} = \boldsymbol{C}_{\rm EFAC} + \boldsymbol{C}_{\rm EQUAD} + \boldsymbol{C}_{\rm ECORR}, \tag{14}$$

where $\boldsymbol{C}_{\rm EFAC}$, $\boldsymbol{C}_{\rm EQUAD}$, and $\boldsymbol{C}_{\rm ECORR}$ are the correlation functions for EFAC, EQUAD, and ECORR parameters, respectively. Explicit expressions for these correlation functions can be found in Ref. [75].

The third term, $\delta\boldsymbol{t}_{\rm SSE}$, is a noise due to inaccuracies of a solar system ephemeris (SSE) which is used to convert observatory TOAs to an inertial frame centered at the solar system barycenter. The SSE noise can seriously affect the upper limits and Bayes factors when searching for stochastic gravitational-wave backgrounds [72]. In our analysis, we use DE436 [87] as the fiducial SSE model. To account for the SSE errors, we employ the physical model BAYESEPHEM introduced in Ref. [72] and implemented in NANOGrav's flagship package ENTERPRISE [88]. The BAYESEPHEM model has eleven parameters, including four parameters which correspond to perturbations in the masses of the outer planets, one parameter describes a rotation rate about the ecliptic pole, and six parameters characterize the corrections to Earth's orbit generated by perturbing Jupiter's average orbital elements [72].

The last term, $\delta\boldsymbol{t}_{\rm SIGW}$, is the observed timing residuals due to the SIGW, which are described by the cross-power spectral density [89]

$$S_{IJ}(f) = \frac{H_0^2}{16\pi^4 f^5}\Gamma_{IJ}(f)\Omega_{\rm GW}(f), \tag{15}$$

where Γ_{IJ} is the Hellings and Downs coefficients [78] measuring the spatial correlation of the pulsars I and J in the array. The expression for $\Omega_{\rm GW}(f)$ is given by Eq. (6).

TABLE II. Parameters and their prior distributions used in the analyses.

Parameter	Description	Prior	Comments
		SIGW signal	
A	GWB strain amplitude	Uniform $[10^{-5}, 10^{0}]$ (upper limits)	
		Log-Uniform $[-5, 0]$ (model comparison)	One parameter for PTA
f_*	Peak frequency	Delta function	Fixed
		White noise	
E_k	EFAC per backend and receiver system	Uniform [0, 10]	Single-pulsar analysis only
Q_k[s]	EQUAD per backend and receiver system	Log-Uniform $[-8.5, -5]$	Single-pulsar analysis only
J_k[s]	ECORR per backend and receiver system	Log-Uniform $[-8.5, -5]$	Single-pulsar analysis only
		Red noise	
$A_{\rm RN}$	Red-noise power-law amplitude	Uniform $[10^{-20}, 10^{-11}]$ (upper limits)	
		Log-Uniform $[-20, -11]$ (model comparison)	One parameter per pulsar
$\gamma_{\rm RN}$	Red-noise power-law spectral index	Uniform [0, 9]	One parameter per pulsar
		BAYESEPHEM	
$z_{\rm drift}$ [rad/yr]	Drift-rate of Earth's orbit about ecliptic z-axis	Uniform $[-10^{-9}, 10^{-9}]$	One parameter for PTA
$\Delta M_{\rm jupiter}$ $[M_\odot]$	Perturbation to Jupiter's mass	$\mathcal{N}(0, 1.55 \times 10^{-11})$	One parameter for PTA
$\Delta M_{\rm saturn}$ $[M_\odot]$	Perturbation to Saturn's mass	$\mathcal{N}(0, 8.17 \times 10^{-12})$	One parameter for PTA
$\Delta M_{\rm uranus}$ $[M_\odot]$	Perturbation to Uranus' mass	$\mathcal{N}(0, 5.72 \times 10^{-11})$	One parameter for PTA
$\Delta M_{\rm neptune}$ $[M_\odot]$	Perturbation to Neptune's mass	$\mathcal{N}(0, 7.96 \times 10^{-11})$	One parameter for PTA
PCA$_i$	Principal components of Jupiter's orbit	Uniform $[-0.05, 0.05]$	Six parameters for PTA

The free parameters for the SIGW are the amplitude A and the peak frequency f_*. For a fixed f_*, the mass of a PBH is given by Eq. (2). In this sense, the free parameter A is directly related to the abundance of PBHs $f_{\rm PBH}$.

For the timing model parameters and TOAs, we use the publicly available data files from the NANOGrav 11-year dataset [56]. To extract information from the data, we perform a Bayesian inference by closely following the procedure in Ref. [72]. The parameters of our model and their prior distributions are presented in Table II. In order to reduce the computational costs, a common strategy is to fix the white noise parameters to their max likelihood values determined from independent single-pulsar analysis, in which only the white and red noises are considered. Fixing white noise parameters can greatly reduce the number of free parameters.

Assuming the $\delta \boldsymbol{t}_{\rm RGP}$ is Gaussian and stationary, for a PTA with M pulsars, the likelihood function can be evaluated as [90]

$$\mathcal{L} = \frac{1}{\sqrt{\det(2\pi\boldsymbol{\Sigma})}} \exp\left(-\frac{1}{2}\mathbf{R}^T\boldsymbol{\Sigma}^{-1}\mathbf{R}\right), \tag{16}$$

where $\mathbf{R} \equiv [\delta \boldsymbol{t}^1_{\rm RGP}, \delta \boldsymbol{t}^2_{\rm RGP}, \ldots, \delta \boldsymbol{t}^M_{\rm RGP}]^T$ is a collection of $\delta \boldsymbol{t}_{\rm RGP}$ for all pulsars, and $\boldsymbol{\Sigma} \equiv \langle \mathbf{R}\mathbf{R}^T \rangle$ is the covariance matrix. Following the common practice in Refs. [86,91,92], we marginalize over the timing model parameter $\boldsymbol{\epsilon}$ when evaluating the likelihood. The likelihood is calculated by using the pulsar timing package ENTERPRISE. To achieve parallel tempering, we use the PTMCMCSampler [93] package to do the Markov chain Monte Carlo sampling.

Given the observational data $\mathcal{D}$, one needs to distinguish two exclusive models: a noise-only model $\mathcal{H}_0$ and a noise-plus-signal model $\mathcal{H}_1$. The model selection is quantified by the Bayes factor

$$B_{10} = \frac{\text{evidence}[\mathcal{H}_1]}{\text{evidence}[\mathcal{H}_0]} = \frac{p(A=0|\mathcal{H}_1)}{p(A=0|\mathcal{D},\mathcal{H}_1)}, \tag{17}$$

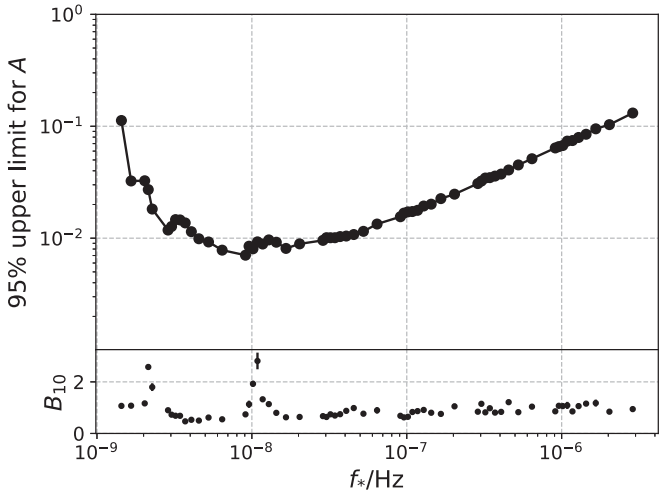

FIG. 1. Top panel: The 95% upper limits on the power spectrum amplitude A of curvature perturbation as a function of the peak frequency f_* from the NANOGrav 11-year dataset. Bottom panel: The corresponding Bayes factors B_{10} as a function of the peak frequency f_*.

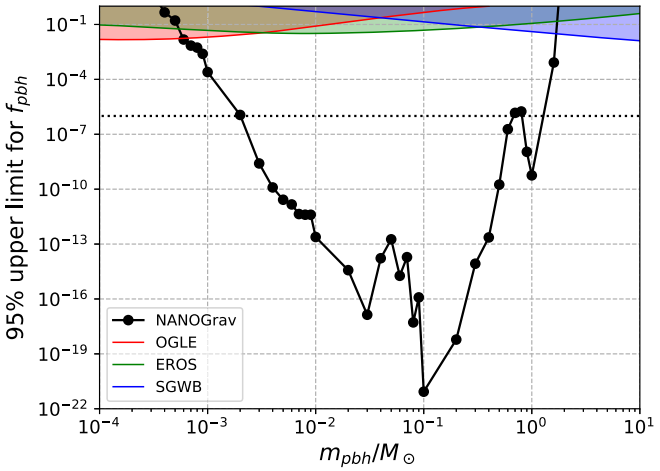

FIG. 2. The 95% upper limits on the abundance of PBHs in DM $f_{\rm PBH}$ as a function of the PBH mass $m_{\rm PBH}$ from the NANOGrav 11-year dataset. Results from OGLE microlensing (OGLE) [23], EROS and MACHO microlensing (EROS) [24], and SGWB [35] are also shown. The horizontal dotted line corresponds to 10^{-6}.

where the numerator and denominator are the prior and posterior probability density of $A = 0$ in the model $\mathcal{H}_1$, respectively. We have used the Savage-Dickey formula [94] to estimate the Bayes factor in Eq. (17).

Results and conclusion.—The upper limits and the Bayes factor for the power spectrum amplitude A as a function of the peak frequency f_* from the NANOGrav 11-year dataset are shown in Fig. 1 at the 95% confidence level. Even though there are two peaks in the Bayes factor distribution, both peak values are smaller than 3, implying the presence of a signal in the data is "not worth more than a bare mention" [95]. Since the Bayes factor B_{10} for each peak frequency is less than 3, it indicates that the data is consistent with containing noise only. The upper limits on the abundance of PBHs in DM $f_{\rm PBH}$ as a function of the PBH mass $m_{\rm PBH}$ are given in Fig. 2 at the 95% confidence level. Note that $m_{\rm PBH}$ is related to f_* by Eq. (2), and $f_{\rm PBH}$ is related to A and $m_{\rm PBH}$ by Eq. (3). Our results imply that the current PTA dataset has already been able to place a stringent constraint on the abundance of PBHs through the SIGWs. According to Fig. 2, the abundance of PBHs is less than 10^{-6} in the mass range of $[2 \times 10^{-3}, 7 \times 10^{-1}] M_\odot$.

In this Letter, we give the first search for the signal of SIGWs inevitably accompanying the formation of PBHs in the NANOGrav 11-year dataset. Since no significant signal is found, we place a 95% upper limit on the amplitude of scalar perturbation over the peak frequency range of $[1.5 \times 10^{-9}, 3 \times 10^{-6}]$ Hz and the abundance of PBHs in the mass range of $[4 \times 10^{-4}, 1.7]\ M_\odot$. In particular, the abundance of PBHs in the mass range of $[2 \times 10^{-3}, 7 \times 10^{-1}]\ M_\odot$ is less than 10^{-6}, which is much better than any other observational constraints in this mass range in the literature. Since the amplitude of SIGWs is roughly determined by the peak amplitude of scalar power spectrum even for the case with an extended mass distribution, a similar constraint on the peak amplitude of scalar power spectrum should be obtained from the NANOGrav 11-yr data, and therefore a stringent constraint on the abundance of PBHs with an extended mass distribution can be also expected. In principle, the exact analysis for the case with an extended mass distribution is model dependent, and will be left for the future.

We acknowledge the use of HPC Cluster of ITP-CAS. This work is supported by grants from NSFC (Grants No. 11975019, No. 11690021, No. 11991052, and No. 11947302), the Strategic Priority Research Program of Chinese Academy of Sciences (Grants No. XDB23000000 and No. XDA15020701), and Key Research Program of Frontier Sciences, CAS, Grant No. ZDBS-LY-7009.

*chenzucheng@itp.ac.cn
†yuanchen@itp.ac.cn
‡Corresponding author.
huangqg@itp.ac.cn

[1] B. P. Abbott *et al.* (LIGO Scientific and Virgo Collaborations), Observation of Gravitational Waves from a Binary Black Hole Merger, Phys. Rev. Lett. **116**, 061102 (2016).
[2] B. P. Abbott *et al.* (LIGO Scientific and Virgo Collaborations), GW151226: Observation of Gravitational Waves from a 22-Solar-Mass binary black hole coalescence, Phys. Rev. Lett. **116**, 241103 (2016).
[3] B. P. Abbott *et al.* (LIGO Scientific and Virgo Collaborations), GW170104: Observation of a 50-solar-mass binary black hole coalescence at Redshift 0.2, Phys. Rev. Lett. **118**, 221101 (2017); Erratum, Phys. Rev. Lett. **121**, 129901 (2018).
[4] B.. P.. Abbott *et al.* (LIGO Scientific and Virgo Collaborations), GW170608: Observation of a 19-solar-mass binary black hole coalescence, Astrophys. J. **851**, L35 (2017).
[5] B. P. Abbott *et al.* (LIGO Scientific and Virgo Collaborations), GW170814: A Three-Detector Observation of Gravitational Waves from a Binary Black Hole Coalescence, Phys. Rev. Lett. **119**, 141101 (2017).
[6] B. P. Abbott *et al.* (LIGO Scientific and Virgo Collaborations), Binary Black Hole Mergers in the First Advanced LIGO Observing Run, Phys. Rev. X **6**, 041015 (2016); Erratum, Phys. Rev. X **8**, 039903 (2018).
[7] B. P. Abbott *et al.* (LIGO Scientific and Virgo Collaborations), GWTC-1: A Gravitational-Wave Transient Catalog of Compact Binary Mergers Observed by LIGO and Virgo During the First and Second Observing Runs, Phys. Rev. X **9**, 031040 (2019).
[8] B. P. Abbott *et al.* (LIGO Scientific and Virgo Collaborations), GW170817: Observation of Gravitational Waves from a Binary Neutron Star Inspiral, Phys. Rev. Lett. **119**, 161101 (2017).
[9] S. Bird, I. Cholis, J. B. Muñoz, Y. Ali-Haïmoud, M. Kamionkowski, E. D. Kovetz, A. Raccanelli, and A. G. Riess, Did LIGO Detect Dark Matter?, Phys. Rev. Lett. **116**, 201301 (2016).

[10] M. Sasaki, T. Suyama, T. Tanaka, and S. Yokoyama, Primordial Black Hole Scenario for the Gravitational-Wave Event GW150914, Phys. Rev. Lett. **117**, 061101 (2016); Erratum, Phys. Rev. Lett. **121**, 059901 (2018).
[11] Z.-C. Chen and Q.-G. Huang, Merger rate distribution of primordial-black-hole binaries, Astrophys. J. **864**, 61 (2018).
[12] S. Hawking, Gravitationally collapsed objects of very low mass, Mon. Not. R. Astron. Soc. **152**, 75 (1971).
[13] B. J. Carr and S. W. Hawking, Black holes in the early Universe, Mon. Not. R. Astron. Soc. **168**, 399 (1974).
[14] P. Ivanov, P. Naselsky, and I. Novikov, Inflation and primordial black holes as dark matter, Phys. Rev. D **50**, 7173 (1994).
[15] J. Yokoyama, Formation of MACHO primordial black holes in inflationary cosmology, Astron. Astrophys. **318**, 673 (1997).
[16] J. Garcia-Bellido, A. D. Linde, and D. Wands, Density perturbations and black hole formation in hybrid inflation, Phys. Rev. D **54**, 6040 (1996).
[17] P. Ivanov, Nonlinear metric perturbations and production of primordial black holes, Phys. Rev. D **57**, 7145 (1998).
[18] M. Kawasaki, T. Takayama, M. Yamaguchi, and J. Yokoyama, Power spectrum of the density perturbations from smooth hybrid new inflation model, Phys. Rev. D **74**, 043525 (2006).
[19] B. J. Carr, K. Kohri, Y. Sendouda, and J. Yokoyama, New cosmological constraints on primordial black holes, Phys. Rev. D **81**, 104019 (2010).
[20] A. Barnacka, J. F. Glicenstein, and R. Moderski, New constraints on primordial black holes abundance from femtolensing of gamma-ray bursts, Phys. Rev. D **86**, 043001 (2012).
[21] H. Niikura *et al.*, Microlensing constraints on primordial black holes with Subaru/HSC Andromeda observations, Nat. Astron. **3**, 524 (2019).
[22] K. Griest, A. M. Cieplak, and M. J. Lehner, New Limits on Primordial Black Hole Dark Matter from an Analysis of Kepler Source Microlensing Data, Phys. Rev. Lett. **111**, 181302 (2013).
[23] H. Niikura, M. Takada, S. Yokoyama, T. Sumi, and S. Masaki, Constraints on Earth-mass primordial black holes from OGLE 5-year microlensing events, Phys. Rev. D **99**, 083503 (2019).
[24] P. Tisserand *et al.* (EROS-2), Limits on the macho content of the galactic halo from the EROS-2 survey of the magellanic clouds, Astron. Astrophys. **469**, 387 (2007).
[25] P. W. Graham, S. Rajendran, and J. Varela, Dark matter triggers of supernovae, Phys. Rev. D **92**, 063007 (2015).
[26] P. Montero-Camacho, X. Fang, G. Vasquez, M. Silva, and C. M. Hirata, Revisiting constraints on asteroid-mass primordial black holes as dark matter candidates, J. Cosmol. Astropart. Phys. 08 (2019) 031.
[27] T. D. Brandt, Constraints on MACHO dark matter from compact stellar systems in ultra-faint Dwarf galaxies, Astrophys. J. **824**, L31 (2016).
[28] D. Gaggero, G. Bertone, F. Calore, R. M. T. Connors, M. Lovell, S. Markoff, and E. Storm, Searching for Primordial Black Holes in the Radio and X-Ray Sky, Phys. Rev. Lett. **118**, 241101 (2017).
[29] Y. Ali-Haïmoud and M. Kamionkowski, Cosmic microwave background limits on accreting primordial black holes, Phys. Rev. D **95**, 043534 (2017).
[30] D. Aloni, K. Blum, and R. Flauger, Cosmic microwave background constraints on primordial black hole dark matter, J. Cosmol. Astropart. Phys. 05 (2017) 017.
[31] B. Horowitz, Revisiting primordial black holes constraints from ionization history, arXiv:1612.07264.
[32] L. Chen, Q.-G. Huang, and K. Wang, Constraint on the abundance of primordial black holes in dark matter from Planck data, J. Cosmol. Astropart. Phys. 12 (2016) 044.
[33] B. P. Abbott *et al.* (LIGO Scientific and Virgo Collaborations), Search for Subsolar-Mass Ultracompact Binaries in Advanced LIGO's First Observing Run, Phys. Rev. Lett. **121**, 231103 (2018).
[34] R. Magee, A.-S. Deutsch, P. McClincy, C. Hanna, C. Horst, D. Meacher, C. Messick, S. Shandera, and M. Wade, Methods for the detection of gravitational waves from subsolar mass ultracompact binaries, Phys. Rev. D **98**, 103024 (2018).
[35] Z.-C. Chen and Q.-G. Huang, Distinguishing primordial black holes from astrophysical black holes by einstein telescope and cosmic explorer, arXiv:1904.02396.
[36] B. P. Abbott *et al.* (LIGO Scientific and Virgo Collaborations), Search for Sub-Solar Mass Ultracompact Binaries in Advanced LIGO's Second Observing Run, Phys. Rev. Lett. **123**, 161102 (2019).
[37] S. Wang, Y.-F. Wang, Q.-G. Huang, and T. G. F. Li, Constraints on the Primordial Black Hole Abundance from the First Advanced LIGO Observation Run Using the Stochastic Gravitational-Wave Background, Phys. Rev. Lett. **120**, 191102 (2018).
[38] K. Tomita, Non-linear theory of gravitational instability in the expanding universe, Prog. Theor. Phys. **37**, 831 (1967).
[39] R. Saito and J. Yokoyama, Gravitational Wave Background as a Probe of the Primordial Black Hole Abundance, Phys. Rev. Lett. **102**, 161101 (2009); Erratum, Phys. Rev. Lett. **107**, 069901 (2011).
[40] S. Young, C. T. Byrnes, and M. Sasaki, Calculating the mass fraction of primordial black holes, J. Cosmol. Astropart. Phys. 07 (2014) 045.
[41] R.-g. Cai, S. Pi, and M. Sasaki, Gravitational Waves Induced by Non-Gaussian Scalar Perturbations, Phys. Rev. Lett. **122**, 201101 (2019).
[42] C. Yuan, Z.-C. Chen, and Q.-G. Huang, Probing primordial-black-hole dark matter with scalar induced gravitational waves, Phys. Rev. D **100**, 081301 (2019).
[43] R.-G. Cai, S. Pi, S.-J. Wang, and X.-Y. Yang, Pulsar timing array constraints on the induced gravitational waves, J. Cosmol. Astropart. Phys. 10 (**2019**) 059.
[44] C. Yuan, Z.-C. Chen, and Q.-G. Huang, Scalar induced gravitational waves in different gauges, Phys. Rev. D **101**, 063018 (2020).
[45] C. Yuan, Z.-C. Chen, and Q.-G. Huang, Log-dependent slope of scalar induced gravitational waves in the infrared regions, Phys. Rev. D **101**, 043019 (2020).
[46] H. Audley *et al.* (LISA Collaboration), Laser interferometer space antenna, arXiv:1702.00786.

[47] G. Hobbs *et al.*, The international pulsar timing array project: Using pulsars as a gravitational wave detector, Classical Quantum Gravity **27**, 084013 (2010).
[48] R. Nan, D. Li, C. Jin, Q. Wang, L. Zhu, W. Zhu, H. Zhang, Y. Yue, and L. Qian, The Five-Hundred-Meter Aperture Spherical Radio Telescope (FAST) project, Int. J. Mod. Phys. D **20**, 989 (2011).
[49] M. Kramer and B. Stappers, Pulsar science with the SKA, Proc. Sci. AASKA14 (**2015**) 036.
[50] K. Inomata, M. Kawasaki, K. Mukaida, Y. Tada, and T. T. Yanagida, Inflationary primordial black holes for the LIGO gravitational wave events and pulsar timing array experiments, Phys. Rev. D **95**, 123510 (2017).
[51] K. Schutz and A. Liu, Pulsar timing can constrain primordial black holes in the LIGO mass window, Phys. Rev. D **95**, 023002 (2017).
[52] N. Orlofsky, A. Pierce, and J. D. Wells, Inflationary theory and pulsar timing investigations of primordial black holes and gravitational waves, Phys. Rev. D **95**, 063518 (2017).
[53] J. A. Dror, H. Ramani, T. Trickle, and K. M. Zurek, Pulsar timing probes of primordial black holes and subhalos, Phys. Rev. D **100**, 023003 (2019).
[54] S. Wang, T. Terada, and K. Kohri, Prospective constraints on the primordial black hole abundance from the stochastic gravitational-wave backgrounds produced by coalescing events and curvature perturbations, Phys. Rev. D **99**, 103531 (2019).
[55] S. Clesse, J. García-Bellido, and S. Orani, Detecting the stochastic gravitational wave background from primordial black hole formation, arXiv:1812.11011.
[56] Z. Arzoumanian *et al.* (NANOGrav Collaboration), The NANOGrav 11-year data set: High-precision timing of 45 millisecond pulsars, Astrophys. J. Suppl. **235**, 37 (2018).
[57] J. M. Bardeen, J. R. Bond, N. Kaiser, and A. S. Szalay, The statistics of peaks of gaussian random fields, Astrophys. J. **304**, 15 (1986).
[58] B. Carr, F. Kuhnel, and M. Sandstad, Primordial black holes as dark matter, Phys. Rev. D **94**, 083504 (2016).
[59] I. Musco, J. C. Miller, and A. G. Polnarev, Primordial black hole formation in the radiative era: Investigation of the critical nature of the collapse, Classical Quantum Gravity **26**, 235001 (2009).
[60] I. Musco, J. C. Miller, and L. Rezzolla, Computations of primordial black hole formation, Classical Quantum Gravity **22**, 1405 (2005).
[61] I. Musco and J. C. Miller, Primordial black hole formation in the early universe: Critical behaviour and self-similarity, Classical Quantum Gravity **30**, 145009 (2013).
[62] T. Harada, C.-M. Yoo, and K. Kohri, Threshold of primordial black hole formation, Phys. Rev. D **88**, 084051 (2013); Erratum, Phys. Rev. D **89**, 029903 (2014).
[63] A. Escrivà, Simulation of primordial black hole formation using pseudo-spectral methods, Phys. Dark Universe **27**, 100466 (2020).
[64] A. Escrivà, C. Germani, and R. K. Sheth, A universal threshold for primordial black hole formation, Phys. Rev. D **101**, 044022 (2020).
[65] M. Maggiore, Gravitational wave experiments and early universe cosmology, Phys. Rep. **331**, 283 (2000).
[66] J. Ramón Espinosa, D. Racco, and A. Riotto, A cosmological signature of the SM Higgs instability: Gravitational waves, J. Cosmol. Astropart. Phys. 09 (2018) 012.
[67] K. Kohri and T. Terada, Semianalytic calculation of gravitational wave spectrum nonlinearly induced from primordial curvature perturbations, Phys. Rev. D **97**, 123532 (2018).
[68] http://nanograv.org.
[69] www.atnf.csiro. au/research/pulsar/ppta.
[70] http://www.epta.eu.org.
[71] K. Aggarwal *et al.*, The NANOGrav 11-year data set: Limits on gravitational waves from individual supermassive black hole binaries, Astrophys. J. **880**, 116 (2019).
[72] Z. Arzoumanian *et al.* (NANOGRAV Collaboration), The NANOGrav 11-year data set: Pulsar-timing constraints on the stochastic gravitational-wave background, Astrophys. J. **859**, 47 (2018).
[73] R. M. Shannon *et al.*, Gravitational-wave limits from pulsar timing constrain supermassive black hole evolution, Science **342**, 334 (2013).
[74] R. van Haasteren *et al.*, Placing limits on the stochastic gravitational-wave background using European Pulsar Timing Array data, Mon. Not. R. Astron. Soc. **414**, 3117 (2011); Erratum, Mon. Not. R. Astron. Soc. **425**, 1597 (2012).
[75] R. Kato and J. Soda, Search for ultralight scalar dark matter with NANOGrav pulsar timing arrays, arXiv:1904.09143.
[76] M. V. Sazhin, Opportunities for detecting ultralong gravitational waves, Sov. Astron. **22**, 36 (1978).
[77] S. L. Detweiler, Pulsar timing measurements and the search for gravitational waves, Astrophys. J. **234**, 1100 (1979).
[78] R. W. Hellings and G. S. Downs, Upper limits on the isotropic gravitational radiation background from pulsar timing analysis, Astrophys. J. **265**, L39 (1983).
[79] R. S. Foster and D. C. Backer, Constructing a pulsar timing array, Astrophys. J. **361**, 300 (1990).
[80] S. R. Taylor, J. R. Gair, and L. Lentati, Weighing the evidence for a gravitational-wave background in the first international pulsar timing array data challenge, Phys. Rev. D **87**, 044035 (2013).
[81] R. van Haasteren and Y. Levin, Understanding and analysing time-correlated stochastic signals in pulsar timing, Mon. Not. R. Astron. Soc. **428**, 1147 (2013).
[82] vallis.github.io/libstempo.
[83] https://bitbucket.org/psrsoft/tempo2.git.
[84] G. Hobbs, R. Edwards, and R. Manchester, TEMPO2, a new pulsar timing package. 1. overview, Mon. Not. R. Astron. Soc. **369**, 655 (2006).
[85] R. T. Edwards, G. B. Hobbs, and R. N. Manchester, Tempo2, a new pulsar timing package. 2. The timing model and precision estimates, Mon. Not. R. Astron. Soc. **372**, 1549 (2006).
[86] R. van Haasteren and M. Vallisneri, New advances in the Gaussian-process approach to pulsar-timing data analysis, Phys. Rev. D **90**, 104012 (2014).
[87] W. M. Folkner and R. S. Park, JPL planetary and Lunar ephemeris DE436, Jet Propulsion Laboratory, 2016.
[88] https://github.com/nanograv/enterprise.
[89] E. Thrane and J. D. Romano, Sensitivity curves for searches for gravitational-wave backgrounds, Phys. Rev. D **88**, 124032 (2013).
[90] J. A. Ellis, X. Siemens, and R. van Haasteren, An efficient approximation to the likelihood for gravitational wave

stochastic background detection using pulsar timing data, Astrophys. J. **769**, 63 (2013).
[91] L. Lentati, P. Alexander, M. P. Hobson, S. Taylor, J. Gair, S. T. Balan, and R. van Haasteren, Hyper-efficient model-independent Bayesian method for the analysis of pulsar timing data, Phys. Rev. D **87**, 104021 (2013).
[92] R. van Haasteren and M. Vallisneri, Low-rank approximations for large stationary covariance matrices, as used in the Bayesian and generalized-least-squares analysis of pulsar-timing data, Mon. Not. R. Astron. Soc. **446**, 1170 (2015).
[93] https://github.com/jellis18/PTMCMCSampler.
[94] J. M. Dickey, The weighted likelihood ratio, linear hypotheses on normal location parameters, Ann. Math. Stat. **42**, 204 (1971).
[95] R. E. Kass and A. E. Raftery, Bayes factors, J. Am. Stat. Assoc. **90**, 773 (1995).